Electronic Supplementary Material (ESI) for Faraday Discussions.

Supporting Information

for

Mechanochemical reaction kinetics scales linearly with impact energy

Leonarda Vugrin,[a,⊥] Maria Carta,[b,⊥] Stipe Lukin,[a] Ernest Meštrović,[c] Francesco Delogu, [b,*] Ivan Halasz [a,*]

[a]Ruđer Bošković Institute, Bijenička c. 54, 10000 Zagreb, Croatia

[b]Department of Mechanical, Chemical and Materials Engineering, University of Cagliari, via Marengo 2, 09123 Cagliari, Italy

[c] Department of Chemistry, Faculty of Science, University of Zagreb, Horvatovac 102a, 10000 Zagreb, Croatia

[⊥]equal contribution

Emails: **francesco.delogu@unica.it**; **ivan.halasz@irb.hr**

1. Experimental

Synthesis. Dibenzoylmethane (Hdbm, 8.97 g, 40 mmol) was dissolved in 100 ml of ethanol with stirring and heating until complete dissolution. Potassium hydroxide (2.24 g, 40 mmol) was dissolved in a water/ethanol mixture and added to the prepared solution of Hdbm. Nickel(II) chloride hexahydrate (4.75 g, 20 mmol) was dissolved in distilled water and added to the alkaline solution of Hdbm. The mixture was heated with stirring until a light green precipitate was observed. About 200 ml of distilled water was added to the solution and placed in an ultrasonic bath. The light green complex of $Ni(dbm)_2(H_2O)_2$ was filtered with suction and dried. To remove water, the dihydrate was suspended in boiling isooctane until the suspension turned dark brown and the resulting brown solid $Ni(dbm)_2$ was filtered with suction and dried.

In situ monitoring and Raman-spectra analysis. For *in situ* Raman monitoring experiments, 200 mg (0.4 mmol) of the brown $Ni(dbm)_2$ was placed in a translucent PMMA vessel of 14 ml internal volume together with one milling ball. Spectra were collected for 1000 ms with a new dark spectrum collected before each data spectrum. Time resolution between spectra was thus 2 seconds. Later on, the Raman spectra were averaged in sets of five spectra, which reduced the total number of experimental Raman spectra by five, reduced time resolution to 10 seconds, but improved the signal-to-noise ratio. Laser power at 785 nm was 485 mW. The total recording time was 45 min (for milling at frequencies 32.5 and 35.0 Hz) or 60 min (27.5 and 30.0 Hz). Reaction profiles were estimated using restrained non-negative least-squares procedure. Each milling experiment was repeated 3 times to yield an average reaction profile for each of the milling conditions.

PMMA jar signal subtraction. We collected Raman spectra of an empty PMMA jar under the same conditions and with the same parameters as we collected the *in situ* Raman spectra for the chemical transformation. In total, we obtained total 900 Raman spectra of an empty jar. For subtraction of the PMMA signal contribution we used the following procedure: First, 75 randomly selected spectra for the empty PMMA jar were averaged and their mean spectrum was scaled and subtracted from a single experimental spectrum. The procedure was repeated for every experimental spectrum. The scale factor was obtained by least-squares minimization of a difference (up to a multiplication factor) between the Raman band in the range 2909 – 2989 cm^{-1} of the experimental and empty PMMA jar spectrum. In other words, we solve the equation $\mathbf{A}x = \mathbf{B}$ for x which is a scale

factor, **A** is a vector of Raman intensities values in range 2909 – 2989 cm^{-1} for empty PMMA jar, and **B** is the vector of Raman intensities values in range 2909 – 2989 cm^{-1} for an experimental spectrum. After obtaining *x* and multiplying with the full empty jar spectrum, such a scaled spectrum was subtracted from the full experimental spectrum.

Baseline correction and normalization. After the PMMA signal subtraction we reduced the Raman spectra to the range 906 – 1670 cm^{-1} where the most prominent changes occurs during the reaction. We then applied asymmetric least-squares algorithm for baseline correction and subsequently normalize the corrected spectra by dividing all spectral points with L1 norm.

Reaction profiles were estimated using restrained non-negative least-squares procedure (implemented through MATLAB lsqnonneg function) and for each experimental spectrum we solved the equation:

$||FX - Y||_2^2$ where $\mathbf{X} \geq 0$, and $\sum x_i = 1$

Where **F** is a matrix of pure components, **X** is a vector corresponding to the mole fractions, and **Y** is a vector of the experimental spectrum. Standard deviations for the derived mole fractions for each experimental spectrum were estimated from the covariance matrix:

$$\mathrm{Cov} = \sigma^2(\mathbf{F}\mathbf{F}^{\mathrm{T}})^{-1}$$

Where σ^2 is the variance of residuals calculated as:

$$\sigma^2 = \frac{e^T e}{n - p}$$

In the above equation **e** is the vector of residuals, *n* is the number of spectral points, and *p* is the number of estimated mole fractions. Since the experiments were repeated, the final reaction profiles were taken as the mean average of several derived profiles. Reaction profiles for all the experiments are given in Figures S1-S3.

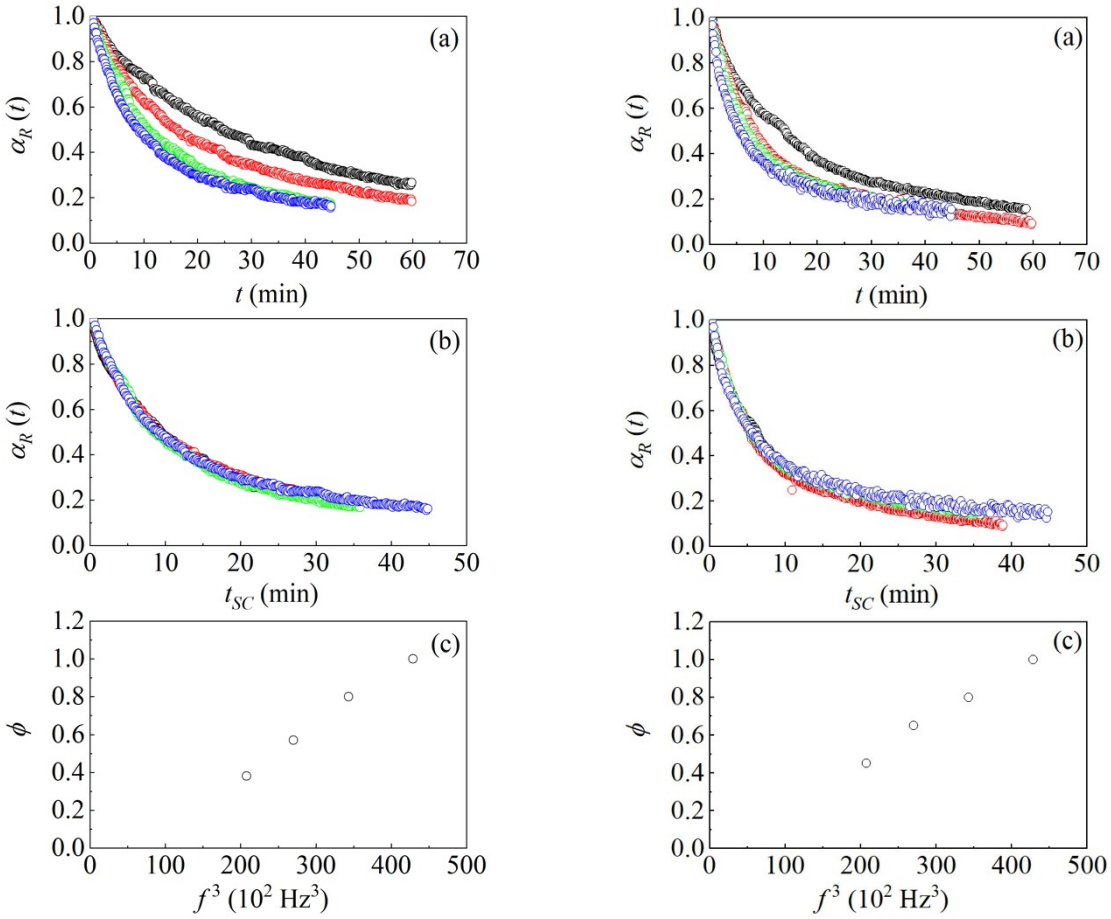

Figure S1. Kinetic curves for one stainless steel milling ball of (left) 8 mm and (right) 10 mm in diameter. (a) The reactant fraction $\alpha_R(t)$, as a function of time, t for milling experiments at four milling frequencies. (b) The reactant fraction $\alpha_R(t)$, as a function of the rescaled time, t_{SC}. (c) The dependence of the scaling parameter, ϕ, with the third powder of the milling frequency. The figure on the left is repeated from the main text for easier comparison.

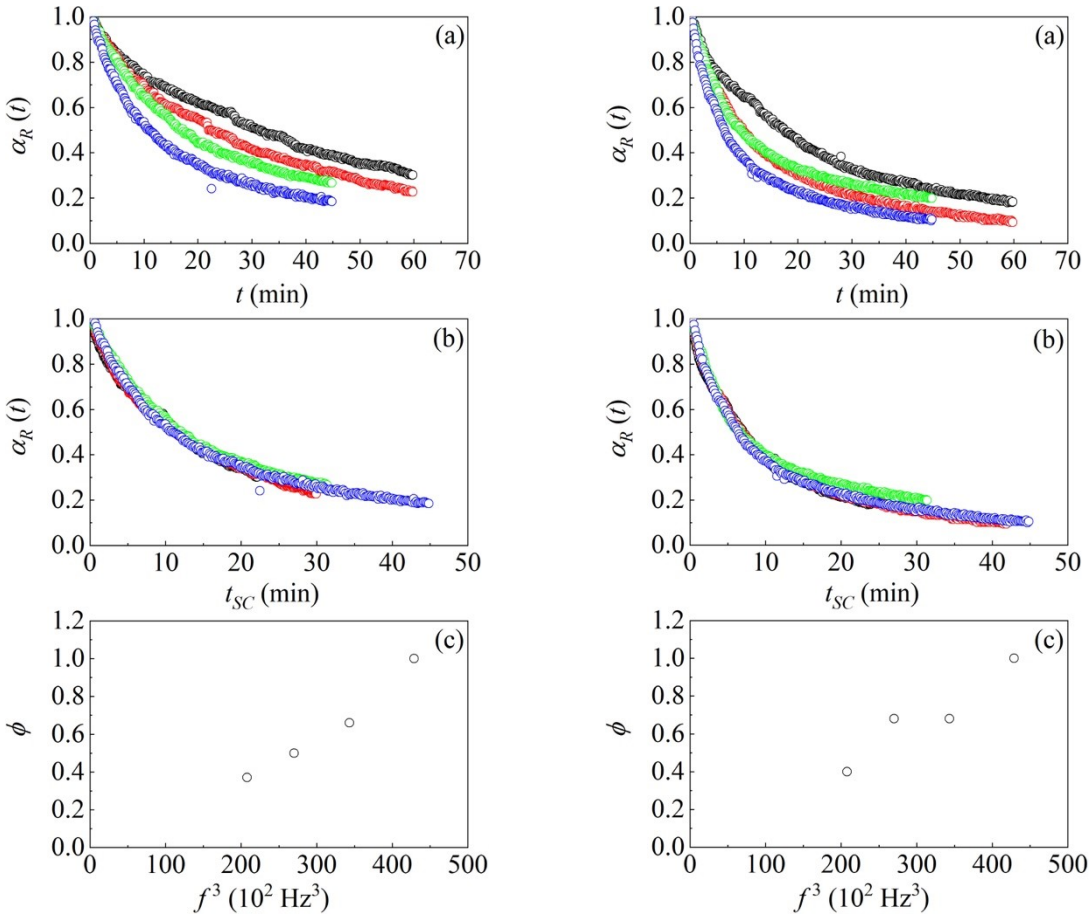

Figure S2. Kinetic curves for one zirconia milling ball of (left) 8 mm and (right) 10 mm in diameter. (a) The reactant fraction $\alpha_R(t)$, as a function of time, t for milling experiments at four milling frequencies. (b) The reactant fraction $\alpha_R(t)$, as a function of the rescaled time, t_{SC}. (c) The dependence of the scaling parameter, ϕ, with the third powder of the milling frequency.

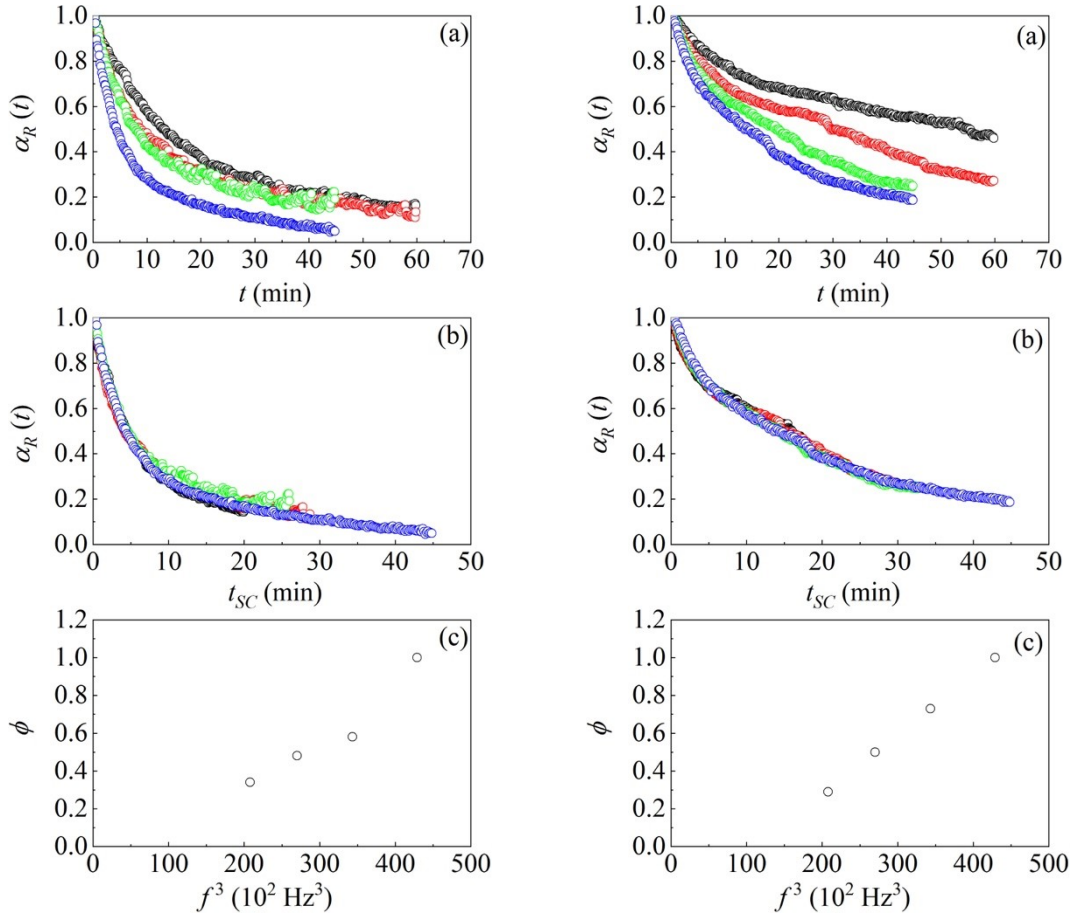

Figure S3. Kinetic curves for (left) one tungsten carbide milling ball of 8 mm and (right) one agate milling ball of 10 mm in diameter. (a) The reactant fraction $\alpha_R(t)$, as a function of time, t for milling experiments at four milling frequencies. (b) The reactant fraction $\alpha_R(t)$, as a function of the rescaled time, t_{SC}. (c) The dependence of the scaling parameter, ϕ, with the third powder of the milling frequency.

3. Kinetic fitting

Kinetic curves have been fitted using Eq. 7 employing Eq. 9.

3.1. ZrO_2 ball

The best fit of kinetic curves resulting from grinding using zirconia balls of both 10 mm and 8 mm diameter are reported.

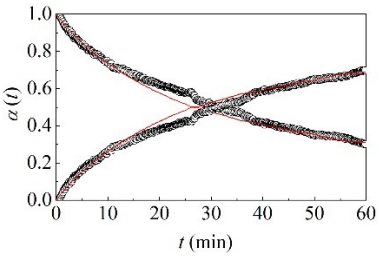

Figure S4. The reactant, $\alpha_R(t)$, and product, $\alpha_p(t)$, volume fraction as a function time, t. Data refer to experiments carried out with a 8-mm ZrO_2 ball at 27.5 Hz. Best- fitted curves are also shown. k_R and k_P values are equal to 0.037 s^{-1} and 0.012 s^{-1}.

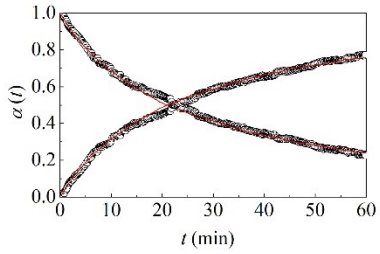

Figure S5. The reactant, $\alpha_R(t)$, and product, $\alpha_p(t)$, volume fraction as a function time, t. Data refer to experiments carried out with a 8-mm ZrO_2 ball at 30 Hz. Best- fitted curves are also shown. k_R and k_P values are equal to 0.047 s^{-1} and 0.017 s^{-1}.

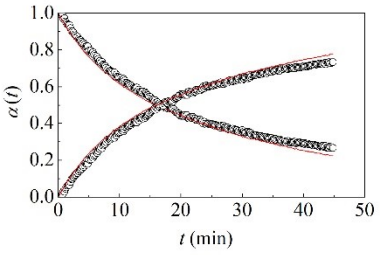

Figure S6. The reactant, $\alpha_R(t)$, and product, $\alpha_p(t)$, volume fraction as a function time, t. Data refer to experiments carried out with a 8-mm ZrO_2 ball at 32.5 Hz. Best- fitted curves are also shown. k_R and k_P values are equal to 0.062 s^{-1} and 0.023 s^{-1}.

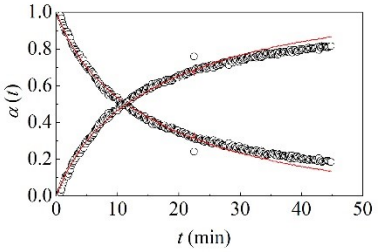

Figure S7. The reactant, $\alpha_R(t)$, and product, $\alpha_p(t)$, volume fraction as a function time, t. Data refer to experiments carried out with a 8-mm ZrO_2 ball at 35 Hz. Best- fitted curves are also shown. k_R and k_P values are equal to 0.087 s^{-1} and 0.035 s^{-1}.

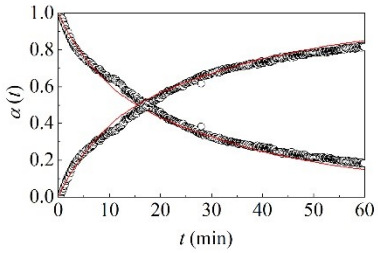

Figure S8. The reactant, $\alpha_R(t)$, and product, $\alpha_p(t)$, volume fraction as a function time, t. Data refer to experiments carried out with a 10-mm ZrO_2 ball at 27.5 Hz. Best- fitted curves are also shown.

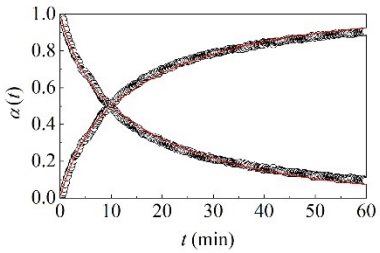

Figure S9. The reactant, $\alpha_R(t)$, and product, $\alpha_p(t)$, volume fraction as a function time, t. Data refer to experiments carried out with a 10-mm ZrO_2 ball at 30 Hz. Best- fitted curves are also shown. k_R and k_P values are equal to 0.102 s^{-1} and 0.037 s^{-1}.

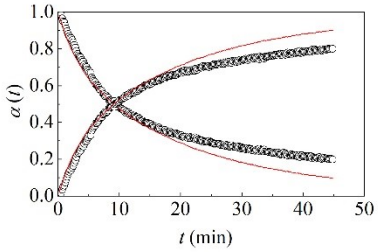

Figure S10. The reactant, $\alpha_R(t)$, and product, $\alpha_p(t)$, volume fraction as a function time, t. Data refer to experiments carried out with a 10-mm ZrO_2 ball at 32.5 Hz. Best- fitted curves are also shown. k_R and k_P values are equal to 0.115 s^{-1} and 0.036 s^{-1}.

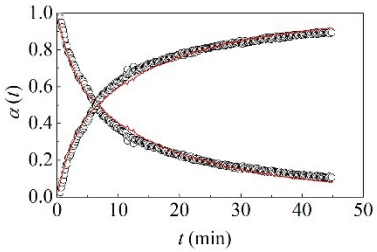

Figure S11. The reactant, $\alpha_R(t)$, and product, $\alpha_p(t)$, volume fraction as a function time, t. Data refer to experiments carried out with a 10-mm ZrO_2 ball at 35 Hz. Best- fitted curves are also shown. k_R and k_P values are equal to 0.17 s^{-1} and 0.043 s^{-1}.

3.2. SS ball

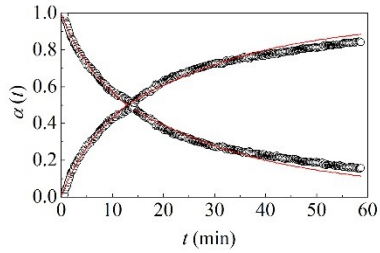

Figure S12. The reactant, $\alpha_R(t)$, and product, $\alpha_p(t)$, volume fraction as a function time, t. Data refer to experiments carried out with a 10-mm SS ball at 27.5 Hz. Best- fitted curves are also shown. k_R and k_P values are equal to 0.075 s^{-1} and 0.03 s^{-1}.

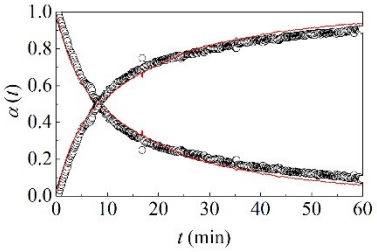

Figure S13. The reactant, $\alpha_R(t)$, and product, $\alpha_p(t)$, volume fraction as a function time, t. Data refer to experiments carried out with a 10-mm SS ball at 30 Hz. Best- fitted curves are also shown. k_R and k_P values are equal to 0.13 s^{-1} and 0.037 s^{-1}.

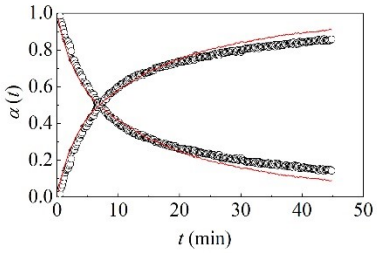

Figure S14. The reactant, $\alpha_R(t)$, and product, $\alpha_p(t)$, volume fraction as a function time, t. Data refer to experiments carried out with a 10-mm SS ball at 32.5 Hz. Best- fitted curves are also shown. k_R and k_P values are equal to 0.165 s^{-1} and 0.037 s^{-1}.

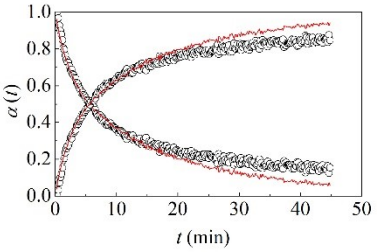

Figure S15. The reactant, $\alpha_R(t)$, and product, $\alpha_p(t)$, volume fraction as a function time, t. Data refer to experiments carried out with a 10-mm SS ball at 35 Hz. Best- fitted curves are also shown. k_R and k_P values are equal to 0.21 s^{-1} and 0.037 s^{-1}.

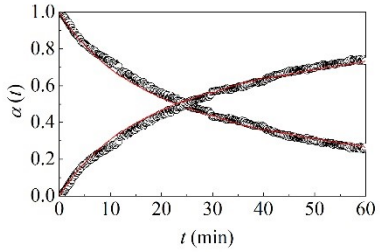

Figure S16. The reactant, $\alpha_R(t)$, and product, $\alpha_p(t)$, volume fraction as a function time, t. Data refer to experiments carried out with a 8-mm SS ball at 27.5 Hz. Best- fitted curves are also shown. k_R and k_P values are equal to 0.045 s^{-1} and 0.014 s^{-1}.

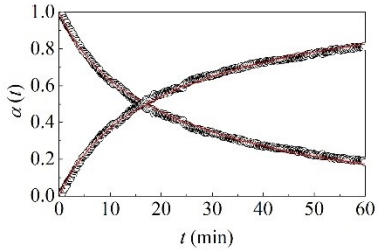

Figure S17. The reactant, $\alpha_R(t)$, and product, $\alpha_p(t)$, volume fraction as a function time, t. Data refer to experiments carried out with a 8-mm SS ball at 30 Hz. Best- fitted curves are also shown. k_R and k_P values are equal to 0.06 s^{-1} and 0.022 s^{-1}.

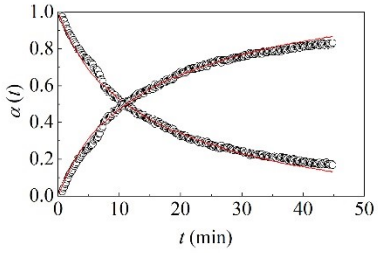

Figure S18. The reactant, $\alpha_R(t)$, and product, $\alpha_p(t)$, volume fraction as a function time, t. Data refer to experiments carried out with a 8-mm SS ball at 32.5 Hz. Best- fitted curves are also shown. k_R and k_P values are equal to 0.089 s^{-1} and 0.036 s^{-1}.

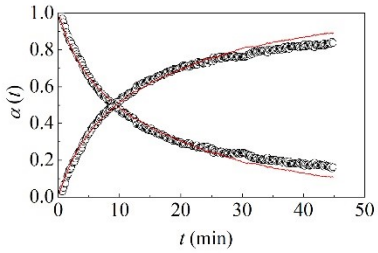

Figure S19. The reactant, $\alpha_R(t)$, and product, $\alpha_p(t)$, volume fraction as a function time, t. Data refer to experiments carried out with a 8-mm SS ball at 35 Hz. Best- fitted curves are also shown. k_R and k_P values are equal to 0.11 s^{-1} and 0.038 s^{-1}.

3.3. Agate ball

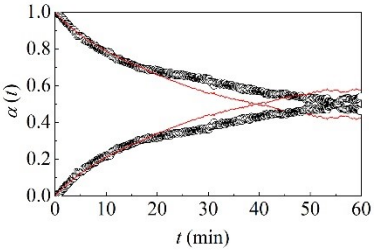

Figure S20. The reactant, $\alpha_R(t)$, and product, $\alpha_p(t)$, volume fraction as a function time, t. Data refer to experiments carried out with a 10-mm Agate ball at 27.5 Hz. Best- fitted curves are also shown. k_R and k_P values are equal to 0.03 s^{-1} and 0.001 s^{-1}.

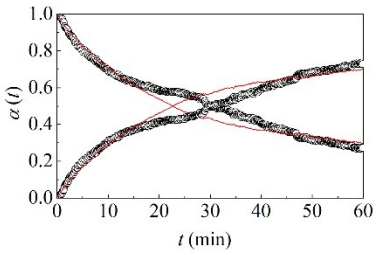

Figure S21. The reactant, $\alpha_R(t)$, and product, $\alpha_p(t)$, volume fraction as a function time, t. Data refer to experiments carried out with a 10-mm Agate ball at 30 Hz. Best- fitted curves are also shown. k_R and k_P values are equal to 0.045 s^{-1} and 0.011 s^{-1}.

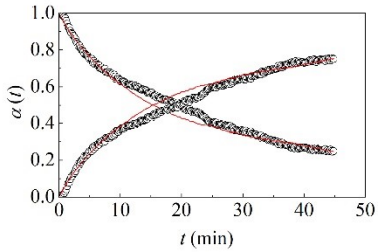

Figure S22. The reactant, $\alpha_R(t)$, and product, $\alpha_p(t)$, volume fraction as a function time, t. Data refer to experiments carried out with a 10-mm Agate ball at 32.5 Hz. Best- fitted curves are also shown. k_R and k_P values are equal to 0.065 s^{-1} and 0.02 s^{-1}.

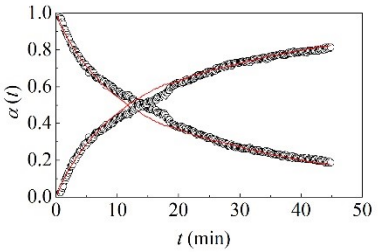

Figure S23. The reactant, $\alpha_R(t)$, and product, $\alpha_p(t)$, volume fraction as a function time, t. Data refer to experiments carried out with a 10-mm Agate ball at 35 Hz. Best- fitted curves are also shown. k_R and k_P values are equal to 0.085 s^{-1} and 0.028 s^{-1}.

3.4. WC ball

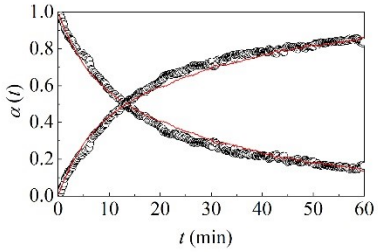

Figure S24. The reactant, $\alpha_R(t)$, and product, $\alpha_p(t)$, volume fraction as a function time, t. Data refer to experiments carried out with a 8-mm WC ball at 27,5 Hz. Best- fitted curves are also shown. k_R and k_P values are equal to 0.08 s^{-1} and 0.024 s^{-1}.

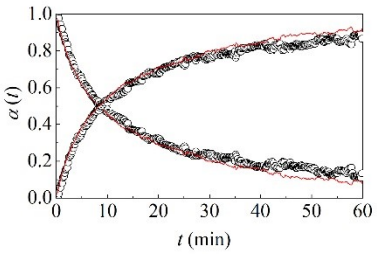

Figure S25. The reactant, $\alpha_R(t)$, and product, $\alpha_p(t)$, volume fraction as a function time, t. Data refer to experiments carried out with a 8-mm WC ball at 30 Hz. Best- fitted curves are also shown. k_R and k_P values are equal to 0.135 s^{-1} and 0.028 s^{-1}.

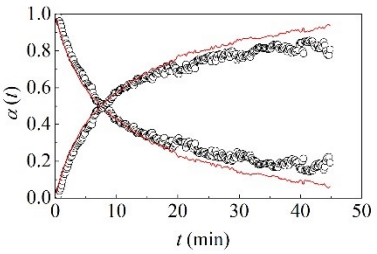

Figure S26. The reactant, $\alpha_R(t)$, and product, $\alpha_p(t)$, volume fraction as a function time, t. Data refer to experiments carried out with a 8-mm WC ball at 32,5 Hz. Best- fitted curves are also shown. k_R and k_P values are equal to 0.14 s^{-1} and 0.043 s^{-1}.

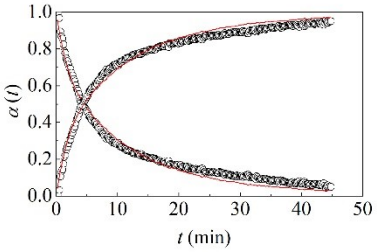

Figure S27. The reactant, $\alpha_R(t)$, and product, $\alpha_p(t)$, volume fraction as a function time, t. Data refer to experiments carried out with a 8-mm WC ball at 35 Hz. Best- fitted curves are also shown. k_R and k_P values are equal to 0.24 s^{-1} and 0.06 s^{-1}.

3. Numerical modelling of ball collisions

The IST636 vibratory ball mill from InSolido Technologies uses an electrical motor to impart simple harmonic motion on the horizontal plane to a vial clamped to a mechanical arm of length R. The vial has cylindrical geometry and rounded bases. Its geometrical center lies slightly off-center the mechanical arm axis. A schematic description is shown in Figure SI.1.

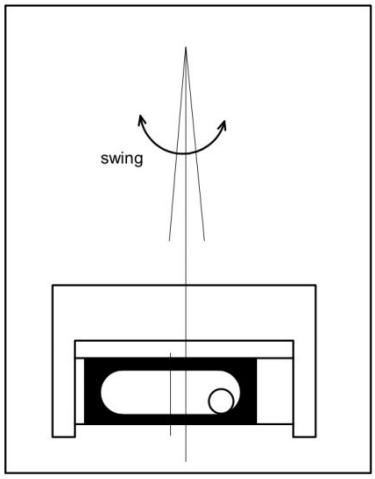

Figure S28. Schematic description of IST636 vibratory ball mill from InSolido Technologies.

The oscillation angle θ varies with time t according to the equation

$$\theta = \theta_{max}\, sin(\omega\, t + \delta) \qquad \text{SI.1}$$

where θ_{max} is the amplitude of the angular motion, $\omega = 2\,\pi\,\nu$ and ν is the milling frequency, whereas δ is a phase factor determined by initial conditions.

We consider two Cartesian reference frames. The inertial one with origin coincident with the fulcrum of the mechanical arm has coordinates $(X;Y;Z)$, whereas the other with coordinates $(x;y;z)$ moves with the vial and has its origin at the intersection point P between the main vial axis and the mechanical arm axis. Inertial and non-inertial Cartesian coordinates of any point in the three-dimensional space are related to each other as expressed by the equation sets

$$X = x\cos\theta + (z + R)\, sin\theta; \qquad \text{SI.2a}$$

$$Y = y; \qquad \text{SI.2b}$$

$$Z = x\sin\theta + (z + R)\, cos\theta; \qquad \text{SI.2c}$$

and

$$x = X\cos\theta - Z\sin\theta; \qquad \text{SI.3a}$$

$$y = Y; \qquad \text{SI.3b}$$

$$z = X \sin\theta + Z \cos\theta - R. \qquad \text{SI.3c}$$

The equations above form the basis for the numerical description of the ball trajectory inside the moving vial. At any given moment, they provide the position of any given point belonging to the vial and, by differentiation with respect to time t, its velocity. Second differentiation with respect to time t yields acceleration.

We note that, compared with the accelerations imparted to the ball by the vial moving at frequencies between 25 Hz and 35 Hz, gravity is negligible. Therefore, the ball motion is governed exclusively by its contacts with the inner vial surfaces. Classical equations of motion for the ball can be solved numerically.

Since we are not interested in reconstructing in detail the impact dynamics, we simply assign impacts a restitution coefficient ranging between 0 (perfectly inelastic impact) and 1 (perfectly elastic impact), and integrate the equations of motion with a time step δt approximately equal to the average impact duration obtained by the Hertz theory of contacts. For the materials used in the present work, Hertz theory indicates that impacts last about 0.01 ms or less. Based on this evidence, we use a δt value of 1×10^{-5}. Equations of motion have been solved using a simple Taylor expansion truncated at the second term.

The ball motion between two consecutive impacts is uniform rectilinear. The non-inertial coordinates of the ball center, $(x_b;y_b;z_b)$, are confined inside the effective volume available to the ball inside the vial. The related geometrical constraints determine the impact conditions. The ball position is checked at any given instant. In case of contact with the vial, the ball velocity is suitably modified. Specifically, the non-inertial velocity component perpendicular to the impact surface is reversed and scaled by the restitution coefficient, e.

The restitution coefficient changes with the material constituting ball and vial. In the presence of powder, it is also affected by the thickness of the powder layer trapped between ball and vial, and its response to dynamic compression. Independent experiments suggest that the milling conditions used in the present work affect the impact elasticity. In general, it can be expected that the impact elasticity degree changes with the hardness of the material constituting the ball.

The numerical simulation of the ball trajectory is carried out by assigning the ball a random position and a random velocity. The system is allowed to reach a stationary state, which typically occurs within 5 s of simulation. For this reason, the first 10 s of simulation are discarded and any statistical study is performed on data obtained after 10 s. A typical 1-s long ball trajectory on the horizontal $(x;z)$ plane is shown in Figure SI.2. It can be seen that, although irregular, the ball motion exhibits remarkable periodicity. The ball moves between the opposite vial ends, often rolling over the

vial surfaces. Preferential paths are evident, mostly associated with the detachment of the ball from the vial surfaces and the subsequent impact.

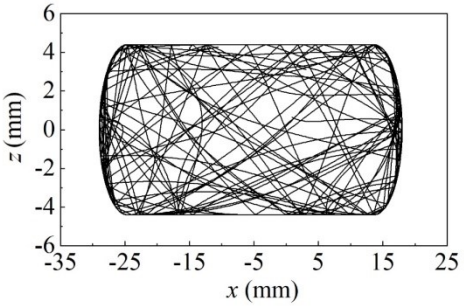

Figure S29. Ball trajectory on horizontal plane. Numerical calculations refer to milling frequency of 27.5 Hz, restitution coefficient of 0.65 and ball diameter equal to 10 mm.

We simulated the milling dynamics for the four selected milling frequencies of 27.5 Hz, 30.0 Hz, 32.5 Hz and 35.0 Hz. The milling dynamics was simulated for 100 s to allow sufficient statistics to evaluate the average impact frequencies, N, and velocities, v. Their values are plotted in Figure SI.3 as a function of the milling frequency, f.

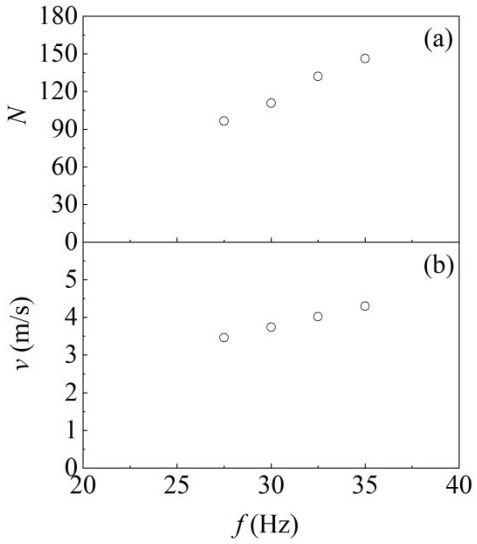

Figure S30. (a) Average impact frequency, N, and (b) average impact velocity, v, as a function of the milling frequency, f. Values refer to calculations performed with restitution coefficient equal to 0.65 and ball diameter equal to 10 mm.